

# GreyReID: A Novel Two-stream Deep Framework with RGB-grey Information for Person Re-identification

LEI QI, The State Key Laboratory for Novel Software Technology, Nanjing University, China

LEI WANG, School of Computing and Information Technology, University of Wollongong, Australia

JING HUO, YINGHUAN SHI, and YANG GAO, The State Key Laboratory for Novel Software Technology, Nanjing University, China

---

In this article, we observe that most false positive images (i.e., different identities with query images) in the top ranking list usually have the similar color information with the query image in person re-identification (Re-ID). Meanwhile, when we use the greyscale images generated from RGB images to conduct the person Re-ID task, some hard query images can obtain better performance compared with using RGB images. Therefore, RGB and greyscale images seem to be complementary to each other for person Re-ID. In this article, we aim to utilize both RGB and greyscale images to improve the person Re-ID performance. To this end, we propose a novel two-stream deep neural network with RGB-grey information, which can effectively fuse RGB and greyscale feature representations to enhance the generalization ability of Re-ID. First, we convert RGB images to greyscale images in each training batch. Based on these RGB and greyscale images, we train the RGB and greyscale branches, respectively. Second, to build up connections between RGB and greyscale branches, we merge the RGB and greyscale branches into a new joint branch. Finally, we concatenate the features of all three branches as the final feature representation for Re-ID. Moreover, in the training process, we adopt the joint learning scheme to simultaneously train each branch by the Independent loss function, which can enhance the generalization ability of each branch. Besides, a global loss function is utilized to further fine-tune the final concatenated feature. The extensive experiments on multiple benchmark datasets fully show that the proposed method can outperform the state-of-the-art person Re-ID methods. Furthermore, using greyscale images can indeed improve the person Re-ID performance in the proposed deep framework.

CCS Concepts: • Computing methodologies → Image representations; Biometrics;

Additional Key Words and Phrases: Person re-identification, greyscale person images, two-stream deep framework

---

This work was supported by Natural Science Foundation of China (No. 61806092 and 61673203), Jiangsu Natural Science Foundation (No. BK20180326), National Key Research and Development Program of China (No. 2019YFC0118300), and Science and Technology Innovation 2030-“New Generation Artificial Intelligence” Major Project (No. 2018AAA0100900 and 2018AAA0100905).

Authors’ addresses: L. Qi, J. Huo, Y. Shi, and Y. Gao (corresponding author), The State Key Laboratory for Novel Software Technology, Nanjing University, Nanjing, China; emails: qilei.cs@gmail.com, {huojing, syh, gaoy}@nju.edu.cn; L. Wang, School of Computing and Information Technology, University of Wollongong, Wollongong, Australia; email: leiw@uow.edu.au.

Permission to make digital or hard copies of all or part of this work for personal or classroom use is granted without fee provided that copies are not made or distributed for profit or commercial advantage and that copies bear this notice and the full citation on the first page. Copyrights for components of this work owned by others than ACM must be honored. Abstracting with credit is permitted. To copy otherwise, or republish, to post on servers or to redistribute to lists, requires prior specific permission and/or a fee. Request permissions from [permissions@acm.org](mailto:permissions@acm.org).

© 2021 Association for Computing Machinery.

1551-6857/2021/04-ART27 \$15.00

<https://doi.org/10.1145/3419439>

**ACM Reference format:**

Lei Qi, Lei Wang, Jing Huo, Yinghuan Shi, and Yang Gao. 2021. GreyReID: A Novel Two-stream Deep Framework with RGB-grey Information for Person Re-identification. *ACM Trans. Multimedia Comput. Commun. Appl.* 17, 1, Article 27 (April 2021), 22 pages.  
<https://doi.org/10.1145/3419439>

---

## 1 INTRODUCTION

Person re-identification (Re-ID) aims at finding the interesting person from a large-scale gallery set that consists of many person images with different illumination, pose, resolution, and background from many non-overlapping camera views [6, 20, 22]. These discrepancies of different camera views result in challenges in person Re-ID. In addition, the similarity among many different person images is also a great challenge for person Re-ID. For example, many person images with different identities could have a similar appearance, especially for the color information.

Many methods have been developed to deal with the above challenges [9, 14, 18, 19, 26, 31, 33, 46, 53]. In recent years, using extra information, such as person attribute [9, 19, 44] and the image-segmentation information [14, 26, 31], has significantly improved the Re-ID performance. Particularly, using image segmentation can effectively reduce the impact of the cluttered background. Besides, to avoid the model over-fitting, some extra images are generated by GANs-based methods to enhance the diversity of training data [18, 27, 53]. Furthermore, the local-based methods can effectively boost the Re-ID performance, which include the part-based methods [28, 29, 36] and the attention-based methods [17, 33, 46]. However, the above methods mainly focus on the challenges caused by the discrepancy of different camera views, which have not paid particular attention to the similarity of the color information among different identities.

In practical applications, there are many similar person images with different identities on the Re-ID dataset, especially in terms of the color information. Thus, for a query image, these similar images with different identities may appear at the top positions of the ranking list. For example, Figure 1 visualizes the ranking list of the PCB model [29], which has obtained the state-of-the-art results on two Re-ID datasets. As seen, for most false positive images in the top ranking list, they have similar color information with query images, which is called the **color over-fitting of person Re-ID** in this article. Thus, many existing methods could overly depend on color information and neglect some structure information in person images.

To solve this issue, we utilize **greyscale images** to conduct the person Re-ID task. Compared with RGB images, greyscale images remove the potentially disturbing color information, and thus using them may make deep models better focus on other information besides the color information, such as structure and texture information. Through the experiments, we find that using greyscale images to conduct the person Re-ID task can generate the complementary results with RGB images, as shown in Figure 2. Some hard query images may fail by using features of RGB images, but utilizing greyscale images can achieve better results. Therefore, we argue that **RGB and greyscale images have the complementarity in the person Re-ID task**. However, since greyscale images could bring the noisy information into the training model, we do not simply use them based on the data-augmentation scheme, which cannot obtain better performance as reported in Table 13. Therefore, we need to design a new deep framework to address this issue.

In this article, to exploit the complementarity between RGB and greyscale images, we propose a **two-stream deep framework** with RGB-grey information for person Re-ID. First, a two-stream network is designed with RGB-greyscale image pairs as inputs. In particular, greyscale images are generated by simply converting RGB images. Then, we fuse the RGB and greyscale branches into a joint branch, which can further extract a more robust feature than RGB and grey features



Fig. 1. Person retrieval samples of the PCB model [29] on CUHK03 and Market1501, respectively. Note that the first image of each row is the query image and other images are “Rank-1 to Rank-10” in the ranking list. The green (red) boxes denote the positive (negative) images with the query image. As seen in this figure, the negative samples in the top positions have similar color information with the query image.

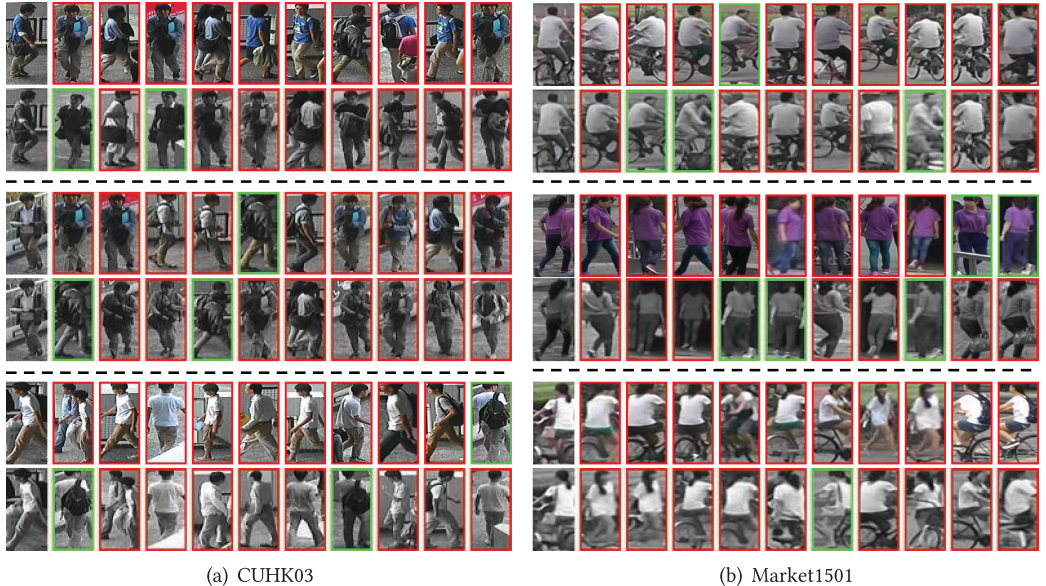


Fig. 2. Person retrieval samples of greyscale and RGB images in the PCB model [29] on CUHK03 and Market1501, respectively. In particular, PCB is trained on greyscale and RGB images, respectively. Top (bottom) of each pair is retrieval samples of RGB (greyscale) images. Note that the first image of each row is the query image and other images are “Rank-1 to Rank-10” in the ranking list. The green (red) boxes denote the positive (negative) images with the query image. As seen in this figure, there is the complementarity between RGB and greyscale images.

alone. Finally, we concatenate the greyscale, RGB and joint features as the final person representation. Moreover, to further enhance the generalization ability of all three branches, an independent loss function is used for each branch in the training stage. In addition, we employ a global loss to further optimize the final concatenated feature. The proposed method can adequately explore the complementary information between RGB and greyscale images to boost the person Re-ID performance.

In summary, we observe that greyscale information has an important role in person Re-ID and put forward an end-to-end deep framework to combine RGB and greyscale information in person image. Our contribution in this work is threefold. First, we find that RGB and greyscale images are complementary in person Re-ID. To the best of our survey, the proposed method is the first to consider the color over-fitting issue in person Re-ID and employs greyscale person images to mitigate this issue. Second, to fully explore the complementary information in RGB and greyscale images, we develop a two-stream network with RGB and greyscale information for person Re-ID, and employ an independent loss function for each branch in the proposed framework. Last, extensive experiments on multiple benchmark datasets demonstrate the efficacy of greyscale images in the person Re-ID task. Furthermore, the proposed method can also obtain competitive performance when compared with the state-of-the-art methods.

The rest of this article is organized as follows: The related work is reviewed in Section 2. The framework proposed in this work is elaborated and discussed in Section 3. Experimental results and analysis are presented in Section 4, and the conclusion is drawn in Section 5.

## 2 RELATED WORK

In this section, we review the most related work with this article in the person Re-ID community.

### 2.1 Person Re-ID with Extra Information

In person Re-ID, extra information, such as person attribute [9, 19, 30] and the image-segmentation information [14, 21, 26, 31], can effectively help to improve the Re-ID performance. Liu et al. [19] present a novel Contextual-attentional Attribute-appearance Network (CA<sup>3</sup>NET) for person Re-ID, which simultaneously exploits the complementarity between semantic attributes and visual appearance. In Reference [9], a novel Attribute-Aware Attention Model (A<sup>3</sup>M) is developed, which can learn local attribute representation and global category representation simultaneously in an end-to-end manner. In addition, due to the diverse background clutters from different camera views, the segmentation information can alleviate background clutters for pedestrian images, and improve the performance of person Re-ID. In Reference [14], the proposed method integrates human semantic parsing in person Re-ID and not only considerably outperforms its counter baseline, but also achieves state-of-the-art performance. Besides, Song et al. [26] introduce the binary segmentation masks to construct synthetic RGB-Mask pairs as inputs, then they design a Mask-guided Contrastive Attention Model (MGCAM) to learn features separately from the body and background regions. Unlike the above methods, considering the color over-fitting issue in person Re-ID, we introduce the greyscale information to enhance the generalization ability of person Re-ID, which is trivially captured by converting RGB images.

### 2.2 Person Re-ID with Extra Images

To enrich training samples, some extra images can be generated by GANs-based methods [18, 34, 48, 52, 53], which can reduce the model over-fitting. Zheng et al. [48] employ GAN [23] to generate unlabeled extra images in the Re-ID task. To use them, a uniform label distribution is assigned to these generated images, which regularizes the supervised model and improves the baseline. Considering the pose variation in different camera views, Liu et al. [18] propose a pose-transferrable

person Re-ID framework that utilizes pose-transferred sample augmentations to enhance Re-ID model training. Besides, person Re-ID also suffers from image style variations caused by different cameras. Zhong et al. [53] implicitly address this problem by learning a camera-invariant descriptor subspace. In particular, the method explicitly considers this challenge by introducing camera style adaptation that can serve as a data augmentation approach that smooths the camera style disparities. Different from the above methods, we introduce the extra greyscale images by converting RGB images directly, which does not need to train extra models, and mitigate the model over-fitting issue from the image color-level view.

### 2.3 The Local-based Person Re-ID

In recent years, the local-based methods can significantly improve the performance of person Re-ID, which include the part-based methods [28, 29, 36, 48] and the attention-based methods [25, 33, 46]. Due to the huge variance of human pose and the misalignment of detected human images, Wei et al. [36] propose a Global-Local-Alignment Descriptor (GLAD) that explicitly leverages the local and global cues in human body to generate a discriminative and robust representation. Su et al. [28] develop a Pose-driven Deep Convolutional (PDC) model to learn improved feature extraction and matching models from end to end, which employs the human part cues to alleviate the pose variations and learn robust feature representations from both the global image and different local parts. Instead of using external cues, such as pose estimation, Sun et al. [29] propose a network named Part-based Convolutional Baseline (PCB) that outputs a convolutional descriptor consisting of several part-level features. Besides, the attention-based model can also locate the local regions. Wang et al. [33] present a novel deep network called Mancs that utilizes the attention mechanism for the person misalignment problem and properly sampling for the ranking loss to obtain a more stable person representation. Zheng et al. [46] propose the Consistent Attentive Siamese Network (CASN), which enforces attention consistency among images of the same identity. Compared with the above methods, the proposed method integrates the different attention regions of greyscale and RGB images to learn the robust feature representations for person Re-ID.

## 3 THE PROPOSED METHOD

In this part, we first present the complementarity between RGB and greyscale images in Section 3.1. Then the proposed two-stream deep framework with RGB-grey information is described in Section 3.2. Last, we further discuss some components of the proposed method in Section 3.3.

### 3.1 The Complementarity between RGB and Greyscale Images

In person Re-ID, most existing methods utilize RGB color images to train and test models. However, these methods may overly depend on the color information (i.e., the color over-fitting). For example, we show person retrieval samples of PCB [29] in the top-10 ranking list in Figure 1. As seen, most of false positive images have similar color information with the query images. Particularly, we remove the color information by making the testing images greyscale. When we evaluate the RGB model (i.e., the model is trained on RGB images) on these greyscale images, mAP decreases by 54.3% (78.5 vs. 24.2), 50.8% (68.5 vs. 17.7), and 44.5% (61.0 vs. 16.5) on Market1501, DukeMTMC-reID, and CUHK03, respectively, as shown in Figure 3 (orange bars vs. blue bars). On one hand, this declares that the color information is important to identify one person. On the other hand, this also implies that the RGB models focus too much on the color information of person images. In this case, using RGB images for person Re-ID may neglect some extra information besides the color information, such as the texture and structure information.

Furthermore, we also observe that RGB and greyscale images for person Re-ID have the complementarity from three different views. First, according to person retrieval samples illustrated in

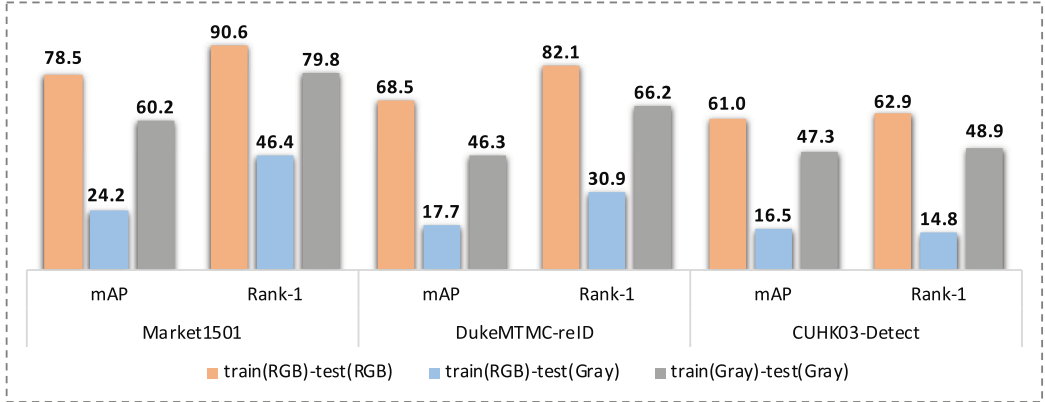


Fig. 3. The evaluation of the greyscale and RGB models on Market1501, DukeMTMC-reID, and CUHK03, respectively. Note that orange (grey) bars denote using RGB (greyscale) images to train and test ResNet-50. Blue bars represent using RGB and greyscale images to train and test the ResNet-50 model, respectively.

Figure 2, by employing greyscale images, some hard query images can achieve better performance than the case of employing RGB images. For example, in Figure 2, some query images cannot find any true positive samples in the top-10 ranking list, while using greyscale images can successfully find some. Second, we also train ResNet-50 [10] on greyscale person images (i.e., the greyscale model). The results are shown in Figure 3 (grey bars). For evaluating the greyscale model on the greyscale data, although the performance has a gap with the RGB model tested on RGB images as shown in Figure 3 (orange bars), it has a great improvement compared with the RGB model evaluated on greyscale data (blue bars in Figure 3). For example, the greyscale model significantly gains 33.4% (79.8 vs. 46.4), 35.3% (66.2 vs. 30.9), and 34.1% (48.9 vs. 14.8) in Rank-1 accuracy on Market1501, DukeMTMC-reID, and CUHK03, respectively. Thus, we can reasonably deduce that the significant improvements could be from the extra information besides the color information, such as the texture or structure information that may not be sufficiently focused by the RGB model. This further confirms the complementarity of RGB and greyscale models. Third, according to feature response maps, we observe that greyscale and RGB images can guide the neural network to focus on different regions. Figure 4 shows feature response maps of greyscale and RGB images in greyscale and RGB models, respectively. As seen, some RGB images neglect the bag regions, while these regions have strong responses in greyscale images.

Considering the complementarity of RGB and greyscale images, our goal is to jointly use greyscale and RGB images to improve the person Re-ID performance by mitigating the color overfitting issue. Particularly, unlike the GANs-based methods that generate extra images, the greyscale images in our method can be trivially obtained by converting RGB images as

$$Grey(i, j) = 0.299 \times R(i, j) + 0.587 \times G(i, j) + 0.114 \times B(i, j), \quad (1)$$

where  $Grey(i, j)$  denotes the pixel value of greyscale images in the  $i$ th row and the  $j$ th column.  $R$ ,  $G$ , and  $B$  are three channels in RGB images. As usual, to use ResNet50, we expand greyscale images to three channels with the same pixel values.

### 3.2 Two-stream Deep Framework with RGB-grey Information

To effectively use greyscale person images, we propose a two-stream deep framework with RGB-grey information for person Re-identification, as illustrated in Figure 5. The detailed information is described as follows.

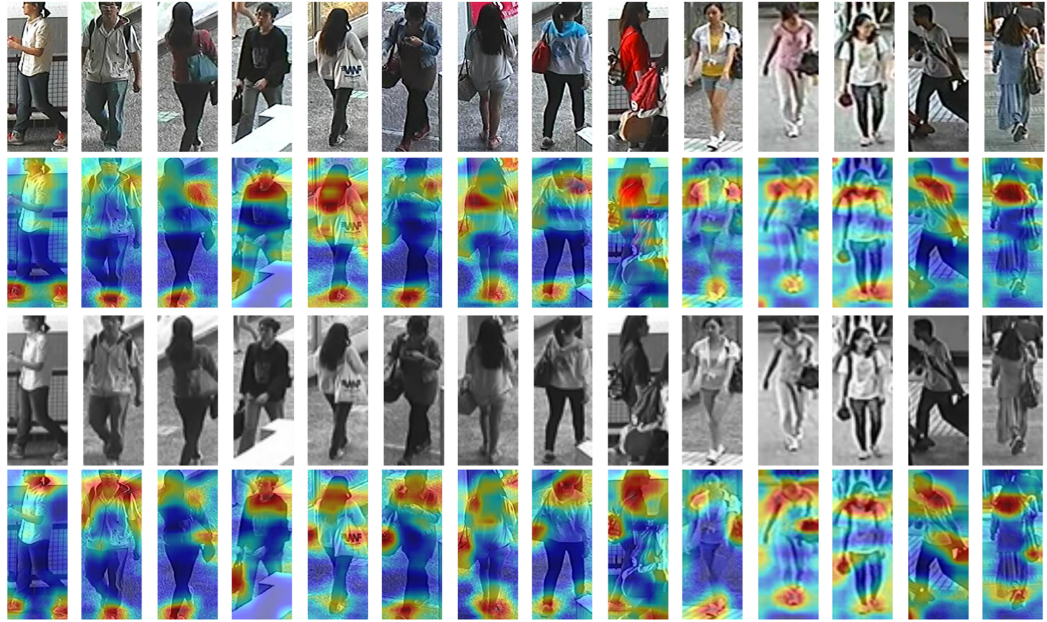


Fig. 4. Feature response maps of the last convolution layer in the greyscale and RGB models on CUHK03. The greyscale (RGB) model represents that ResNet-50 is trained on greyscale (RGB) images. The response map of each person image is calculated by the mean of all feature maps. First and third rows denote the RGB and greyscale images, respectively, and second and fourth rows are their corresponding feature response maps.

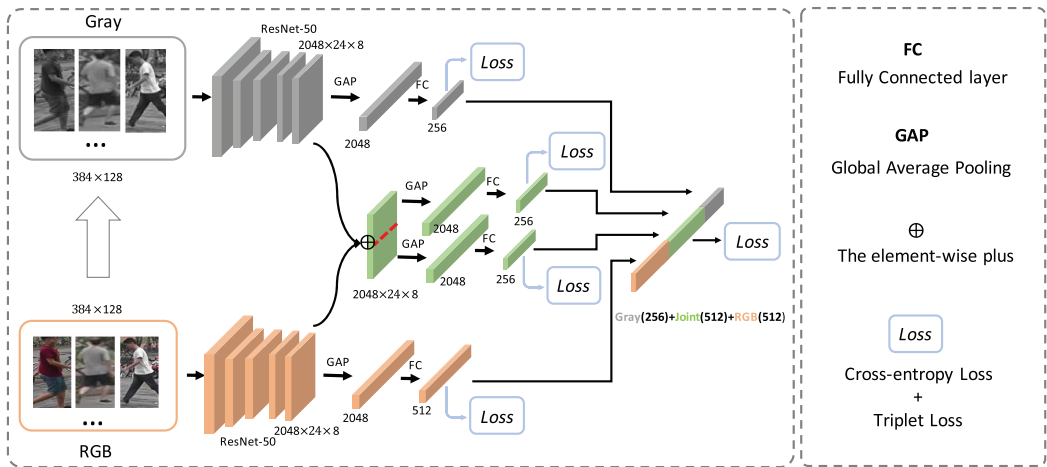


Fig. 5. Illustration of the proposed two-stream deep framework with RGB-grey information. First, we develop a two-stream network for the RGB and greyscale branches. Then, we fuse the two branches into a joint branch. In particular, in the joint branch, we divide the fusion tensor into two parts. Last, we concatenate the features of all branches as the testing feature for Re-ID. During training, we jointly optimize all branches in the proposed framework by the loss of each branch and the global losses in an end-to-end manner.

**The Network Framework.** In this article, we develop a two-stream deep learning framework to fuse RGB and greyscale feature representations, whose backbones are the pre-trained ResNet-50 on ImageNet [5]. In our framework, we first feed RGB images to the RGB branch, and convert RGB images to greyscale images that are fed into the greyscale branch. Second, in the last convolutional layer of ResNet-50, we merge the tensors of the greyscale and RGB branches into a new joint branch to connect them. Particularly, for the joint branch, we adopt the **part-based scheme** to divide the tensor into two parts, whose effectiveness has been validated in the literature [28, 29, 36]. Concretely, given a joint tensor  $T_{joint} \in \mathbb{R}^{2048 \times 24 \times 8}$ , we divide it into two single non-overlapping sub-tensors (i.e.,  $T_{sub1}$  and  $T_{sub2} \in \mathbb{R}^{2048 \times 12 \times 8}$ ). Then, the **global average pooling** (GAP) is employed in all branches. After this, we add a fully connected (FC) layer to form the feature representation of each branch. Finally, we concatenate the features of all branches as the testing feature for Re-ID. In particular, in each branch, we use an independent loss function to train the proposed model simultaneously. Besides, a global loss function is used to fine-tune the concatenated feature, which can further boost the person representation discrimination. In this work, we set 256-, 512-, and 512-d (dimensional) features for the greyscale, RGB, and joint branches, respectively.

**Loss Function.** In person Re-ID, the existing methods construct the classification [4, 16, 39, 43] or discrimination [2, 3, 32, 41] tasks to train deep models. In particular, the effectiveness of simultaneously optimizing the classification and discrimination tasks is demonstrated in Reference [49]. For example, in the discrimination task, the loss function (e.g., contrastive loss [8] or triplet loss [11]) directly calculates the Euclidean distance between two embeddings. In the classification task, the input is independent to each other. But there is implicit relationship between the learned embeddings built by the cross-entropy loss. Thus, we incorporate this joint task to optimize the proposed network. The loss function of the proposed method consists of a cross-entropy loss and a triplet loss with hard sample mining [11]. For the cross-entropy loss of the classification task, it can be defined as

$$\mathcal{L}_{Cross}(X, Y) = - \sum_{i=1}^N \sum_{c=1}^C \delta(y_i - c) \log p(c|x_i), \quad (2)$$

where  $\delta(\cdot)$  is the Dirac delta function. For a sample  $x_i$  belonging to the  $y_i$ -th person class,  $p(c|x_i)$  denotes its predicted probability for the  $c$ th person class.  $N$  is the batch size, and  $C$  represents the total number of person classes.

In each batch, we randomly select  $P$  persons and each person has  $K$  images.  $N = P \times K$  is the total number of images in a batch. The triplet loss with hard sample mining can be described as

$$\mathcal{L}_{Triplet}(X, Y) = \underbrace{\sum_{i=1}^P \sum_{a=1}^K}_{\text{one batch}} \left[ m + l(x_a^i) \right]_+, \quad (3)$$

where

$$l(x_a^i) = \overbrace{\max_{p=1 \dots K} D(f(x_a^i), f(x_p^i))}^{\text{hardest positive}} - \overbrace{\min_{\substack{n=1 \dots K \\ j \neq i}} D(f(x_a^i), f(x_n^j))}^{\text{hardest negative}}, \quad (4)$$

and  $m$  denotes the margin.  $f(x_a^i)$  is the feature of sample  $x_a^i$  and  $D(\cdot, \cdot)$  indicates Euclidean distance.

In summary, the loss function of each branch can be written as

$$\mathcal{L}(X, Y) = \mathcal{L}_{Cross}(X, Y) + \lambda \mathcal{L}_{Triplet}(X, Y), \quad (5)$$

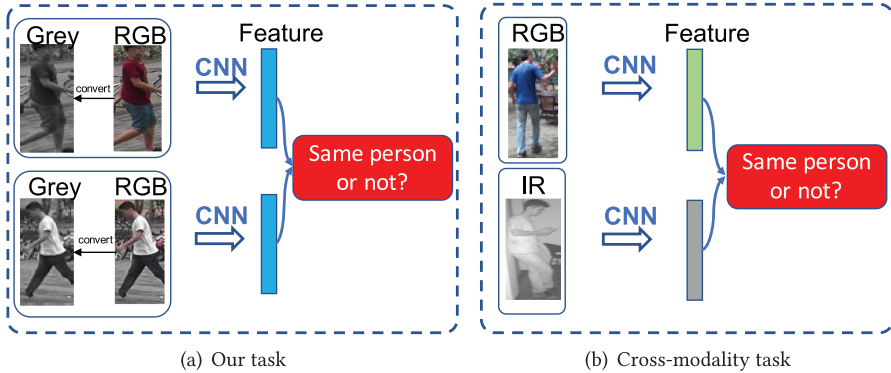


Fig. 6. Comparison between our task and the cross-modality task in References [37, 38, 42]. Note that one feature is produced by using “two” images (i.e., one RGB image and its corresponding greyscale image) in our task. Differently, one feature is generated by using “one” image (i.e., one RGB image or one IR image) in the cross-modality task.

where  $\lambda$  is the hyper-parameter, which is employed to trade off the two losses. In our framework, each branch has an independent loss. Besides, we also utilize a global loss to further fine-tune the concatenated features consisting of the greyscale, RGB, and joint features, as shown in Figure 5.

### 3.3 Discussion

**Why does the proposed framework not use the adaptive weight fusion scheme?** To obtain better joint tensor, we investigate different tensor fusion schemes in our framework, which include element-wise plus, element-wise multiply, concatenated operation, and the adaptive weighting scheme. However, through our experiments, the performance of these tensor fusion schemes does not have enough difference. The main reason is that jointly optimizing the independent loss function of each branch can obtain robust features from all branches. Moreover, the global loss function has been able to automatically adjust the importance of the greyscale, RGB, and joint features in the concatenated feature representation. In some sense, this is equivalent to having an adaptive weighting method for the greyscale, RGB, and joint branches in the proposed framework.

**Why does the proposed framework not use the part-based scheme in other branches?** In our framework, we only employ the part-based scheme in the joint branch. Since the joint branch is the fused part of the greyscale and RGB branches, using the part-based scheme in the joint branch not only improves the performance of the joint branch, but also helps to improve the generalization ability of the RGB and greyscale branches. This has been validated in our experiments. In practice, we also test the case of using the part-based scheme to the RGB branch. However, it cannot bring a significant improvement with respect to our design.

**The difference between the proposed method and the cross-modal method.** Our method is fundamentally different from these cross-modality methods in References [37, 38, 42]. Concretely, we aim to address the conventional person Re-ID task (i.e., the “same-modality” image matching, that is, verifying whether two RGB images belong to the same or different persons). Our framework only employs greyscale images to further boost the generalization ability of the extracted features. Differently, the methods in References [37, 38, 42] deal with the “cross-modality” task (i.e., verifying whether one RGB image and one IR image belong to the same or different identities), as illustrated in Figure 6. Moreover, in our framework, we generate the feature representation for each person by using both its raw RGB image and its corresponding greyscale image. Differently, the cross-modality task extracts IR and RGB image features independently (i.e., one feature

is produced from either one IR image or one RGB image), as shown in Figure 6. In addition, since our goal is not to match RGB images and greyscale images, these methods in References [37, 38, 42] is not suitable to solve our task.

## 4 EXPERIMENTS

In this part, we first introduce the experimental datasets and settings in Section 4.1. Then, we compare the proposed method with baseline and the state-of-the-art methods in Sections 4.2 and 4.3, respectively. To validate the effectiveness of various components in the proposed framework, we conduct ablation studies in Section 4.4. Last, we further analyze the property of the proposed network in Section 4.5.

### 4.1 Datasets and Settings

We evaluate our approach on four large-scale datasets: Market1501 [45], DukeMTMC-reID (Duke) [24, 48], CUHK03-NP [50], and MSMT17 [35]. **Market1501** contains 1,501 persons with 32,668 images from six cameras. Among them, 12,936 images of 751 identities are used as training set. For evaluation, there are 3,368 and 19,732 images in the query set and the gallery set, respectively. **DukeMTMC-reID** has 1,404 persons from eight cameras, with 16,522 training images, 2,228 queries, and 17,661 gallery images. **CUHK03-NP** is a new training-testing split protocol for CUHK03. CUHK03 [15] datasets contain two subsets that provide labeled and detected (from a person detector) person images. The detected CUHK03 set includes 7,365 training images, 1,400 query images, and 5,332 gallery images. The labeled set contains 7,368 training, 1,400 query, and 5,328 gallery images, respectively. The new protocol in Reference [50] splits the training and testing sets into 767 and 700 identities. **MSMT17** is collected from a 15-camera network deployed on campus. The training set contains 32,621 images of 1,041 identities. For evaluation, 11,659 and 82,161 images are used as query and gallery images, respectively. For all datasets, we employ CMC accuracy and mAP for Re-ID evaluation [45]. On Market1501, there are single- and multi-query evaluation protocols. We use the more challenging single-query protocol in our experiments.

In the training process, we set  $P$  and  $K$  to 32 and 4, respectively. The margin of triplet loss,  $m$ , is 0.3. The proposed model is trained with the SGD optimizer in a total of 300 epochs. The initial learning rate is set to 0.01 and decreases to 0.001 and 0.0001 at the 100th and 200th epochs, respectively. During training, the input images are resized to  $384 \times 128$  and then pre-processed by random horizontal flip, normalization, and random erasing [51]. Particularly, all experiments in this article utilize the same setting on all datasets.

Note that the **baseline** model in this experiment represents the pre-trained ResNet-50 [10] on ImageNet [5] with the loss in Equation (5). Particularly, for fair comparison, we set different feature dimensions in the baseline model for different experiments. Baseline-grey and Baseline-rgb denote that the baseline model is trained on greyscale and RGB images, respectively.

### 4.2 Comparison with the Baseline

In this section, we compare the proposed methods and the baseline method, as shown in Figure 7. 1,280-d features are extracted for all methods. Particularly, we conduct the baseline method on greyscale and RGB images, respectively. First, fusing RGB and greyscale features can achieve better results than the features of RGB or greyscale images alone. As seen in Figure 7, when compared with Baseline-rgb, our method can significantly improve mAP by 7.1% (85.6 vs. 78.5), 8.0% (76.5 vs. 68.5), and 8.9% (69.9 vs. 61.0) on Market1501, DukeMTMC-reID, and CUHK03-NP-detect, respectively. This validates the effectiveness of the proposed two-stream deep framework. Second, using greyscale images only to conduct the Re-ID task has poor performance compared with employing RGB images. This can be excerpted, because the color information is also important to

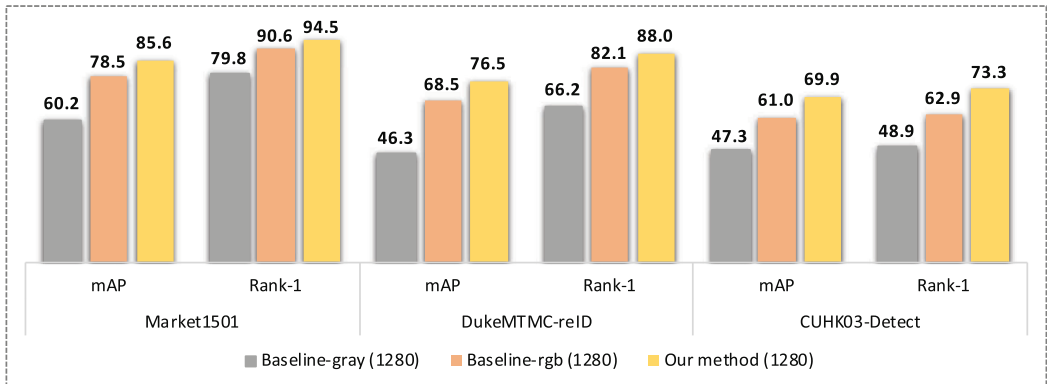


Fig. 7. Comparison of the baseline and our method on Market1501, DukeMTMC-reID, and CUHK03-NP, respectively. Particularly, the baseline model is trained on grey and RGB images, respectively. Note that all methods extract 1,280-dimensional features.

identify a person. Therefore, the proposed framework also utilizes the RGB branch to extract color information.

#### 4.3 Comparison with the State-of-the-art Methods

We compare the proposed methods with the state-of-art methods including attribute-based person Re-ID (A<sup>3</sup>M [9], AANet [30], CA<sup>3</sup>NET [19], MHN-6 [1], CAMA [40], IANet [12]), segmentation-based methods (MGCAM [26], MaskReID [21], SPReID [14]), GANs-based methods (Pose-transfer [18], CamStyle+RE [53], JDGL [47]), part-based methods (PDC [36], GLAD [28], PCB+RPP [29], P<sup>2</sup>-Net [7]), and attention-based methods (Mancs [33], CASN [46]) on Market1501, Duke, CUHK03-NP, and MSMT17, respectively. The experimental results are reported in Tables 1, 2, and 3. Compared with A<sup>3</sup>M [9], CA<sup>3</sup>NET [19], MGCAM [26], and SPReID [14], which use extra information such as person attribute or the image-segmentation information, the proposed method achieves considerable improvement on all datasets. In particular, compared with SPReID, which uses the ResNet-152 as the backbone, our method still can improve mAP by 2.2% (85.6 vs. 83.4) and 3.2% (76.5 vs. 73.3) on Market-1501 and Duke, respectively. Although Pose-transfer [18] and CamStyle+RE [53] generate many extra images to alleviate the model overfitting, they still show an inferior performance to our method. For example, on CUHK03-Detect and CUHK03-Label, the gap between Pose-transfer and our method is about 30% in both mAP and Rank-1 accuracy. The effectiveness of part-based methods (PDC [36], GLAD [28], PCB+RPP [29]) and attention-based methods (Mancs [33], CASN [46]) has been validated in recent years. Compared with these methods, our method can still achieve the competitive results on all datasets. Particularly, on MSMT17, the proposed method improves PCB by 11.8% (55.0 vs. 43.2) and 8.3% (78.6 vs. 70.3) in mAP and Rank-1 accuracy, respectively. These results well demonstrate the effectiveness and advantage of the proposed method by smartly integrating the greyscale and color information of person images.

#### 4.4 Ablation Studies

To adequately validate the effectiveness of the proposed method, we remove the global loss to train the model with the one-part scheme (i.e., without the part-based scheme in the proposed network) and the two-part scheme, respectively. We report the feature combination results of different branches on Market1501, Duke, CUHK03, and MSMT17, as shown in Table 4. “Baseline-grey”

Table 1. Comparison with the State-of-the-art Methods on Market1501 and DukeMTMC-reID, Respectively

Methods	Market1501		DukeMTMC-reID	
	mAP	Rank-1	mAP	Rank-1
A <sup>3</sup> M [9]	69.0	86.5	70.2	84.6
CA <sup>3</sup> NET [19]	80.0	93.2	70.2	84.6
AA-Net [30]	82.5	93.9	72.6	86.4
MHN-6 (IDE) [1]	83.6	93.6	75.2	87.5
CAMA [40]	84.5	<b>94.7</b>	72.9	85.8
IANet [12]	83.1	94.4	73.4	87.1
MGCAM [26]	74.3	83.8	-	-
MaskReID [21]	75.4	90.4	61.9	78.9
SPReID [14]	83.4	93.7	73.3	86.0
P <sup>2</sup> -Net [7]	83.4	94.0	70.8	84.9
Pose-transfer [18]	68.9	87.7	56.9	78.5
CamStyle+RE [53]	71.6	89.5	57.6	78.3
PDC [36]	63.4	84.1	-	-
GLAD [28]	73.9	89.9	-	-
PCB [29]	77.3	92.4	65.3	81.9
PCB+RPP [29]	81.6	93.8	69.2	83.3
Mancs [33]	82.3	93.1	71.8	84.9
CASN [46]	82.8	94.4	73.7	87.7
GreyReID (ours)	<b>85.6</b>	94.5	<b>76.5</b>	<b>88.0</b>

"-" denotes that the result is not provided. The best performance is shown in **bold**.

Table 2. Comparison with the State-of-the-art Methods on CUHK03-NP

Methods	CUHK03-Detect		CUHK03-Label	
	mAP	Rank-1	mAP	Rank-1
MGCAM [26]	46.9	46.7	50.2	50.1
Pose-transfer [18]	38.7	41.6	42.0	45.1
P <sup>2</sup> -Net [7]	64.2	71.6	69.2	75.8
PCB [29]	54.2	61.3	-	-
PCB+RPP [29]	56.7	62.8	-	-
CAMA [40]	64.2	66.6	66.5	70.1
MHN-6 (IDE) [1]	61.2	67.0	65.1	69.7
Mancs [33]	60.5	65.5	63.9	69.0
CASN [46]	64.4	71.5	68.0	73.7
GreyReID (ours)	<b>69.9</b>	<b>73.3</b>	<b>73.9</b>	<b>76.6</b>

The results are reported on both the labeled and detected CUHK03 set. "-" denotes that the result is not provided. The best performance is shown in **bold**.

and "Baseline-rgb" denote that the baseline model is trained on greyscale and RGB images, respectively. For a fair comparison, we set the baseline model to have the same feature dimension with the RGB and greyscale branches in our framework, respectively. Moreover, we concatenate the features of "Baseline-grey" and "Baseline-rgb" to generate new features (Baseline-grey+rgb") to

Table 3. Comparison with the State-of-the-art Methods on MSMT17

Methods	MSMT2017			
	mAP	Rank-1	Rank-5	Rank-10
PDC [36]	29.7	58.0	73.6	79.4
GLAD [28]	34.0	61.4	76.8	81.6
PCB [29]	43.2	70.3	82.9	86.7
IANet [12]	46.8	75.5	85.5	88.7
JDGL [47]	52.3	77.2	87.4	90.5
GreyReID (ours)	<b>55.0</b>	<b>78.6</b>	<b>88.3</b>	<b>91.2</b>

In this table, we report Rank-1, 5, 10 of CMC accuracy and mAP. “-” denotes that the result is not provided. The best performance is shown in **bold**.

Table 4. Performance of the Feature Combination of Different Branches on Market1501, DukeMTMC-reID (Duke), CUHK03-NP-Detect (CHUK03), and MSMT17, Respectively

	Different branches	Market1501		Duke		CUHK03		MSMT17	
		mAP	Rank-1	mAP	Rank-1	mAP	Rank-1	mAP	Rank-1
Baseline	Baseline-grey(256)	57.0	78.7	43.8	63.7	41.2	42.5	26.1	52.1
	Baseline-rgb(512)	77.8	90.6	68.4	83.0	58.0	61.4	44.3	69.6
	Baseline-grey+rgb	<b>81.8</b>	<b>91.9</b>	<b>70.7</b>	<b>84.3</b>	<b>62.8</b>	<b>65.5</b>	<b>49.0</b>	<b>74.1</b>
One-part	Grey(256)	59.0	80.1	46.2	66.4	44.7	46.8	26.5	52.8
	RGB(512)	79.2	90.7	70.0	84.1	61.0	64.6	45.8	70.4
	Joint(512)	82.4	92.4	71.8	85.1	64.1	67.6	50.6	75.0
	Grey+Joint	80.6	92.1	68.5	82.2	62.4	66.4	47.3	73.5
	RGB+Joint	82.5	92.3	72.8	<b>85.4</b>	64.7	68.4	50.7	74.5
	Grey+RGB	83.1	92.8	72.6	85.0	65.6	69.1	50.7	75.5
	Grey+RGB+Joint	<b>83.5</b>	<b>93.0</b>	<b>73.1</b>	85.2	<b>66.2</b>	<b>69.6</b>	<b>51.6</b>	<b>75.9</b>
Two-part	Grey(256)	59.5	79.8	46.2	67.9	46.2	48.6	27.2	53.1
	RGB(512)	80.0	91.3	71.0	84.4	62.8	67.2	46.2	70.8
	Joint(512)	84.3	<b>94.2</b>	74.9	87.0	67.9	71.4	53.2	77.4
	Grey+Joint	83.5	93.6	73.2	86.7	67.3	71.1	51.9	76.9
	RGB+Joint	85.0	94.1	75.8	<b>87.8</b>	69.1	72.4	53.8	77.3
	Grey+RGB	83.7	93.4	73.9	87.3	67.7	71.4	52.0	76.6
	Grey+RGB+Joint	<b>85.3</b>	94.1	<b>75.9</b>	<b>87.8</b>	<b>69.6</b>	<b>73.1</b>	<b>54.5</b>	<b>78.4</b>

Note that in this table, “+” denotes the concatenated operation. Two-part (one-part) indicates the proposed framework with (without) the part-based scheme in the joint branch. The best performance is **bold**.

conduct person Re-ID. Besides, we also validate the efficacy of the loss function in our framework, as reported in Tables 5 and 6.

**Effectiveness of each branch in the proposed network.** In Table 4, “Baseline-grey+rgb” improves “Baseline-rgb” by 4.0% (81.8 vs. 77.8), 2.3% (70.7 vs. 68.4), 4.8% (62.8 vs. 58.0), and 4.7% (49.0 vs. 44.3) in mAP on Market1501, Duke, CUHK03, and MSMT17, respectively. Besides, in our framework, the concatenated feature of the RGB and greyscale branches (“Grey+RGB”) can also enhance the performance when compared with the single RGB branch (“RGB”) for both the one-part and two-part schemes. This demonstrates the effectiveness of greyscale branch in the proposed framework. Moreover, the joint branch can achieve better performance than both the greyscale and RGB branches. This further confirms the effectiveness of fusing the RGB

Table 5. Evaluation of Different Components in the Loss Function on Market1501 and DukeMTMC-reID

Loss Function	Market1501		DukeMTMC-reID	
	mAP	Rank-1	mAP	Rank-1
only $l_{triplet}$ in Equation (5)	75.6	89.6	66.1	81.7
only $l_{cross}$ in Equation (5)	83.8	93.7	73.4	86.7
$l_{cross} + l_{triplet}$	<b>85.6</b>	<b>94.5</b>	<b>76.5</b>	<b>88.0</b>

Table 6. Evaluation of the Branch and Global Losses in Our Framework on Market1501, DukeMTMC-reID (Duke), CUHK03-NP-Detect, and MSMT17, Respectively

Different losses	Market1501		Duke	
	mAP	Rank-1	mAP	Rank-1
w/o branch loss	79.1	91.1	69.5	82.9
w/o global loss	85.3	94.1	75.9	87.8
GreyReID (ours)	<b>85.6</b>	<b>94.5</b>	<b>76.5</b>	<b>88.0</b>

Different losses	CUHK03-NP-Detect		MSMT17	
	mAP	Rank-1	mAP	Rank-1
w/o branch loss	58.4	60.9	44.8	69.8
w/o global loss	69.6	73.1	54.5	78.4
GreyReID (ours)	<b>69.9</b>	<b>73.3</b>	<b>55.0</b>	<b>78.6</b>

“w/o global loss” (“w/o branch loss”) denotes that our framework without the global loss (the losses of all branches). The best performance is **bold**.

and greyscale branches. Particularly, compared with “Joint,” “Grey+Joint” is slightly poorer in all experiments. This is because (i) the joint feature has contained the greyscale information; (ii) although the greyscale information is important for Re-ID, it also introduces some noises.

**Effectiveness of the part-based scheme.** As shown in Table 4, using the part-based scheme not only improves the performance of the joint branch, but also enhances the generalization ability of the RGB and greyscale branches on most datasets. For example, for Grey+RGB+Joint, the two-part method can gain 1.8% (85.3 vs. 83.5), 2.8% (75.9 vs. 73.1), 3.4% (69.6 vs. 66.2), and 2.9% (54.5 vs. 51.6) in mAP on Market1501, Duke, CUHK03, and MSMT17, respectively.

**Effectiveness of joint learning framework.** First, jointly learning RGB and greyscale task is effective to improve the performance of both the greyscale and RGB branches. For example, both “Grey” and “RGB” have some improvements when compared with “Baseline-grey” and “Baseline-rgb,” respectively. For the one-part scheme, compared with “Baseline-rgb,” the performance of the RGB branch in our framework can gain 1.4% (79.2 vs. 77.8), 1.6% (70.0 vs. 68.4), 3.0% (61.0 vs. 58.0), and 1.5% (45.8 vs. 44.3) in mAP on Market1501, Duke, CUHK03, and MSMT17, respectively. Moreover, when using the two-part scheme in our framework, the improvements become more significant. Second, through concatenating the features of all branches, we can obtain the more robust feature representation for Re-ID. As shown in Table 4, “Grey+RGB+Joint” consistently outperforms other feature combinations on most datasets.

**Evaluation of the loss function.** To validate the effectiveness of jointly optimizing the classification and discrimination tasks, we separately use the cross-entropy loss and the triplet loss to train the proposed network on CUHK03, as reported in Table 5. As seen, the joint loss functions can achieve the best performance. Besides, we also validate the effectiveness of using

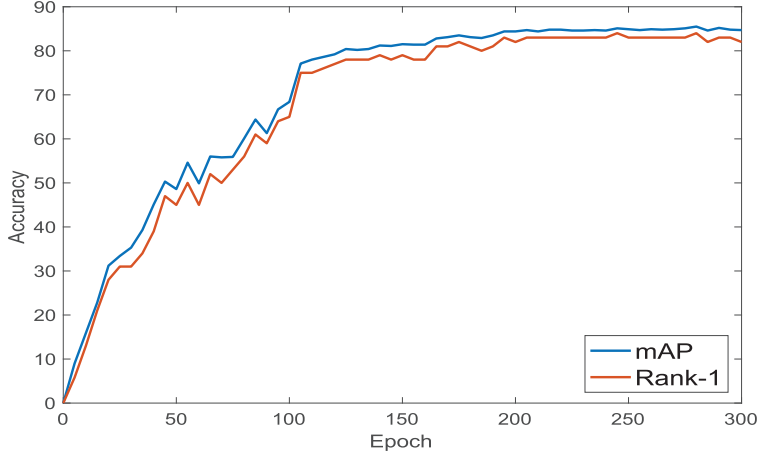


Fig. 8. Convergence curves of the proposed method on MSMT17.

Table 7. Evaluation on Various  $\lambda$  on Market1501 and DukeMTMC-reID

$\lambda$	Market1501		DukeMTMC-reID	
	mAP	Rank-1	mAP	Rank-1
only $l_{triplet}$	75.6	89.6	66.1	81.7
only $l_{cross}$ ( $\lambda = 0$ )	83.8	93.7	73.4	86.7
$\lambda = 0.2$	83.9	93.4	74.2	86.2
$\lambda = 0.5$	84.7	93.9	75.2	87.4
$\lambda = 0.8$	85.4	94.3	75.9	87.0
$\lambda = 1.0$	<b>85.6</b>	<b>94.5</b>	<b>76.5</b>	<b>88.0</b>
$\lambda = 1.5$	85.5	94.1	75.7	86.9
$\lambda = 2.0$	84.6	93.3	74.4	87.1

the independent loss in all branches. We remove the losses of all branches and the global loss from the proposed framework, respectively, which are “w/o branch loss” and “w/o global loss” in Table 6. As seen, “w/o branch loss” has the poorest performance on all datasets. This confirms that the loss in each branch is crucial to fully optimize the proposed network. In addition, using global loss can further boost the robustness of the concatenated feature.

#### 4.5 Further Analysis

**Algorithm Convergence.** To investigate the convergence of our algorithm, we record the mAP and Rank-1 accuracy of the proposed method during the iteration on a validated set of MSMT17 in Figure 8. As seen, we can observe that our proposed method can almost converge after 200 epochs.

**The sensitiveness of parameter.** We conduct the experiment with various  $\lambda$  in Equation (5) to validate the sensitiveness of the parameter, as reported in Table 7. According to the experimental results, we observe that (i) using cross-entropy loss only can obtain better performance than using triplet loss only. This demonstrates the importance of cross-entropy loss in our case. (ii) Using them together can consistently bring more improvement by increasing the value of  $\lambda$ . However, when giving too much attention on the triplet loss (i.e.,  $\lambda > 1$ ), the performance will decrease.

Table 8. Evaluation of Different Inputs in the Proposed Framework on Market1501, DukeMTMC-reID (Duke), CUHK03-NP-Detect (CHUK03), and MSMT17, Respectively

Input	Market1501		Duke		CUHK03		MSMT17	
	mAP	Rank-1	mAP	Rank-1	mAP	Rank-1	mAP	Rank-1
Baseline	78.5	90.6	68.5	82.1	61.0	62.9	44.3	69.3
RGB-RGB pair	85.1	94.0	75.7	87.5	69.6	72.4	53.6	77.3
RGB-grey pair	<b>85.6</b>	<b>94.5</b>	<b>76.5</b>	<b>88.0</b>	<b>69.9</b>	<b>73.3</b>	<b>55.0</b>	<b>78.6</b>

The best performance is **bold**.

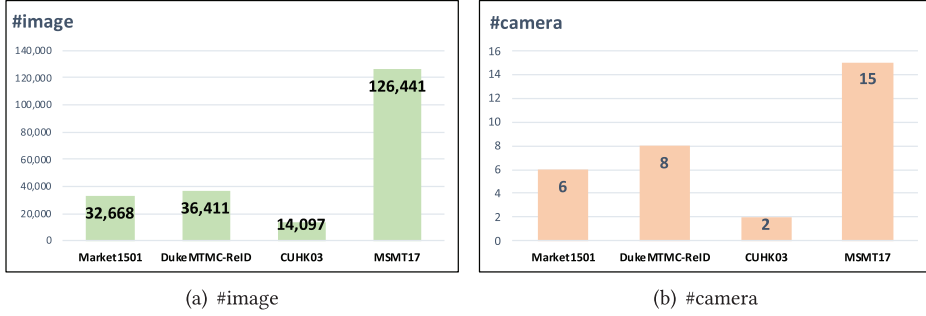


Fig. 9. The numbers of cameras and images on the four benchmark datasets.

**The evaluation of different inputs in the proposed framework.** To further validate the efficacy of greyscale images, we utilize the RGB-RGB pair and the RGB-grey pair as the input of the proposed network, respectively. Note that all settings are the same in this experiment. The experimental results are reported in Table 8. As seen, using the RGB-grey pair as input can achieve a consistent improvement on all datasets. For example, on existing largest person Re-ID dataset (i.e., MSMT17), the RGB-grey pair gains 1.4% (55.0 vs. 53.6) and 1.3% (78.6 vs. 77.3) in mAP and Rank-1 accuracy. Please note that our work consists of two key contributions: First, compared with the baseline in Table 8, which only has an RGB-image input (i.e., without using either the proposed modules of our framework or the greyscale-image input), our framework, regardless of using an RGB-Grey pair or an RGB-RGB pair, can significantly increase the person Re-ID performance, which validates its efficacy. Particularly, the effectiveness of each module in our framework has been validated in the ablation studies of our article. Second, the proposed “RGB-RGB pair” in Table 8 means that the two input branches of our framework are both set as RGB images. That is, we purposely replace the greyscale image in the upper branch with its original RGB image to demonstrate the advantage of using the former. We observe that “RGB-Grey pair” consistently outperforms “RGB-RGB pair” on all the benchmark datasets. Particularly, the most obvious gain is achieved on the dataset MSMT17. As shown in Figure 9, MSMT17 is much larger than the rest three datasets in terms of the number of both cameras and images, and is therefore closer to real scenarios. In this sense, although the improvement of “RGB-Grey pair” over “RGB-RGB pair” is not that significant on these smaller-scale datasets, its significant improvement on MSMT17 clearly shows the superiority and potential for more challenging person Re-ID settings.

**Comparison of different image types.** We also replace the greyscale images by the HSV images. As seen in Table 9, using the HSV images cannot bring improvement when compared with the greyscale images, because an HSV image still contains both color and greyscale information as an RGB image does. As a result, it will be affected in a similar manner as an RGB image in

Table 9. Comparison between Different Image Types on Four Datasets

Image Type	Market1501		DukeMTMC-reID		CUHK03-Detect		MSMT17	
	mAP	Rank-1	mAP	Rank-1	mAP	Rank-1	mAP	Rank-1
Grey+RGB	<b>85.6</b>	<b>94.5</b>	<b>76.5</b>	<b>88.0</b>	<b>69.9</b>	<b>73.3</b>	<b>55.0</b>	<b>78.6</b>
HSV+RGB	83.6	93.5	73.9	86.2	63.6	67.1	49.5	72.6

Table 10. Comparison of Different Color to Greyscale Conversion Methods on Four Datasets

Image Type	Market1501		DukeMTMC-reID		CUHK03-Detect		MSMT17	
	mAP	Rank-1	mAP	Rank-1	mAP	Rank-1	mAP	Rank-1
Grey (ours)	85.6	94.5	76.5	88.0	69.9	73.3	55.0	78.6
Grey-avg	85.8	94.3	76.0	87.8	69.6	72.4	54.8	78.0

Note that “Grey-avg” denotes the average weight setting.

Table 11. Evaluation on Different Backbones on Four Datasets

Backbone	Market1501		DukeMTMC-reID		CUHK03-Detect		MSMT17	
	mAP	Rank-1	mAP	Rank-1	mAP	Rank-1	mAP	Rank-1
Resnet-50	85.6	94.5	76.5	88.0	69.9	73.3	55.0	78.6
Resnet-101	<b>87.9</b>	<b>94.8</b>	<b>78.6</b>	<b>89.3</b>	<b>73.5</b>	<b>77.1</b>	<b>59.1</b>	<b>81.3</b>

terms of the inaccuracy of color information in discriminating some person images. The proposed framework only retains greyscale information and combines it with an RGB image, which can better mitigate the above issue. This has been well verified by the experimental result in Table 9.

**Evaluation of different color to greyscale conversion methods.** The weight setting in our article considers the different human perception/sensibility towards these three colors, which is also used in a popular python toolbox “Pillow”.<sup>1</sup> Following the way of generating greyscale images by “Pillow,” we give the weight (i.e., R -> 0.299; G -> 0.587 and B -> 0.114) in our article. In addition, we also utilize the arithmetical average of R, G, and B to convert RGB images to greyscale images and employ them in our experiments, as reported in Table 10. Overall, the average weight setting is slightly poor when compared with our method.

**The evaluation on different backbones and various dimensions of features.** We also evaluate two ResNet-related backbones in our framework, as reported in Table 11. According to these results, we observe that using a deeper network can enhance the generalization ability of our method. Please note that to have a fair comparison to the state-of-the-art methods, which mostly utilize ResNet-50 as the backbone, we report all experimental results based on ResNet-50 in our article. In addition, we also assess our method with various-dimensional features and report experimental results in Table 12. As seen, the low-dimensional feature (e.g., 192) has poor performance. When the dimension is over 1,024, the performance tends to be stable.

**The evaluation on data augmentation with greyscale images.** To investigate this issue, we specifically leverage the greyscale images in the way of data augmentation and obtain results in Table 13. Note that “RGB:Grey” indicates the ratio between RGB and greyscale images in a training set. For example, for the “1:0.05,” we randomly choose 5% RGB images to convert them into the

<sup>1</sup><https://pillow.readthedocs.io/en/stable/>.

Table 12. Evaluation on Various Feature Dimensions on Four Datasets

RGB+Grey+Joint	Market1501		DukeMTMC-reID	
	mAP	Rank-1	mAP	Rank-1
64+64+64=192	81.1	91.3	71.1	84.4
128+128+256=512	85.0	93.8	75.1	87.3
256+256+512=1,024	85.8	<b>94.6</b>	76.0	87.5
256+512+512=1,280	<b>86.0</b>	94.5	75.8	<b>88.1</b>
512+256+512=1,280	85.6	94.5	<b>76.5</b>	88.0
512+512+512=1,536	85.8	94.3	75.9	86.8

RGB+Grey+Joint	CUHK03-Detect		MSMT17	
	mAP	Rank-1	mAP	Rank-1
64+64+64=192	65.3	67.9	47.3	71.9
128+128+256=512	70.0	72.9	53.4	77.3
256+256+512=1,024	69.7	73.3	<b>55.0</b>	78.4
256+512+512=1,280	<b>70.6</b>	<b>74.8</b>	54.9	<b>78.6</b>
512+256+512=1,280	69.9	73.3	<b>55.0</b>	<b>78.6</b>
512+512+512=1,536	69.8	73.6	54.5	78.4

Note that “RGB+Grey+Joint” denotes the dimensions of the RGB branch, the greyscale branch and the joint branch in our framework, respectively.

Table 13. Results of the Data Augmentation Based on Greyscale Images on Four Datasets

RGB: Grey	Market1501		DukeMTMC-reID		CUHK03-Detect		MSMT17	
	mAP	Rank-1	mAP	Rank-1	mAP	Rank-1	mAP	Rank-1
1 : 0	78.5	90.6	68.5	82.1	61.0	62.9	44.3	69.3
1 : 0.05	78.5	90.9	68.3	82.2	58.9	61.7	44.8	70.1
1 : 0.10	77.7	90.8	67.9	82.3	58.1	60.9	44.9	70.4
1 : 0.25	75.6	90.2	64.2	80.6	55.7	59.7	43.8	69.8
1 : 1	68.7	86.6	54.7	73.8	47.8	51.3	37.0	64.7

Note that “RGB:Grey” denotes the ratio between RGB and greyscale images in a training set.

greyscale images and use all RGB images and these greyscale images to train the model together. From these experimental results, we can see that it is not effective to simply use the greyscale image via data augmentation due to the noisy information from the greyscale image. In other words, different from our proposed framework, the conventional framework cannot effectively explore the complementarity between greyscale images and RGB images via the data-augmentation scheme. Therefore, we develop a novel deep framework to handle the issue.

**The evaluation of different fusion schemes.** As discussed in Section 3.3, we also investigate different tensor fusion schemes in our framework, which include element-wise plus, element-wise multiply, concatenated operation, and the adaptive weighting method. Particularly, for the concatenated operation, we also employ the SE-block [13] to compress the channels. The experimental results are reported in Table 14. In addition, to implement the adaptive weighting method, we embed a weighted network into the proposed framework, which consists of two FC layers that are simultaneously trained with the proposed framework. Given an RGB tensor  $T_{rgb} \in \mathbb{R}^{2048 \times 24 \times 8}$  or a greyscale tensor  $T_{grey} \in \mathbb{R}^{2048 \times 24 \times 8}$ , the input is the 2,048-d feature from GAP of  $T_{rgb}$  or  $T_{grey}$ , and output is the weight value for greyscale or RGB tensors, respectively. We employ softmax to normalize them (i.e.,  $w_{rgb}$  and  $w_{grey}$ ), and generate the joint tensor

Table 14. Evaluation of Different Fusion Schemes on Market1501 and DukeMTMC-reID, Respectively

Methods	Market1501		DukeMTMC-reID	
	mAP	Rank-1	mAP	Rank-1
Concatenate	85.5	94.2	76.2	87.9
Concatenate+SE	85.5	94.1	75.5	87.1
Multiply	<b>85.8</b>	94.3	76.4	<b>88.2</b>
Adaptive weight	85.6	<b>94.5</b>	75.7	87.1
Plus (ours)	85.6	<b>94.5</b>	<b>76.5</b>	88.0

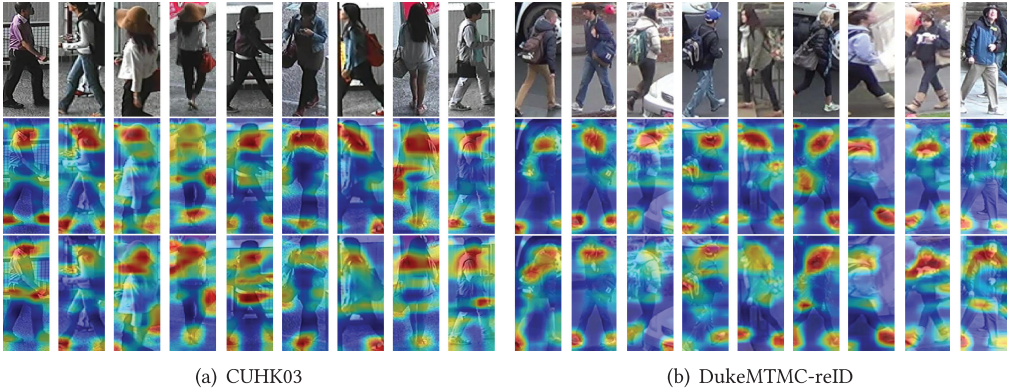


Fig. 10. Feature response maps of the last convolutional layer in the RGB and greyscale branches of the proposed method, respectively. Note that these images are from the testing set of CUHK03 and DukeMTMC-reID. Top denotes RGB images. Middle and bottom are feature response maps of the greyscale and RGB branches, respectively. Note the complementarity between them.

$T_{joint} = w_{grey} \times T_{grey} + w_{rgb} \times T_{rgb}$ . This method is implemented by ourselves. As seen in Table 14, all results do not achieve significantly better performance than the proposed one. This is because the joint learning framework, using the independent loss in each branch and a global loss for the concatenated feature, has guaranteed the proposed network can obtain the robust features for person Re-ID, as discussed in Section 3.3.

**The visualization of the RGB and greyscale branches.** To further validate the complementarity between RGB and greyscale images, we visualize feature maps of the last convolutional layer in the greyscale and RGB branches of the proposed method, as shown in Figure 10. Since the conventional methods mainly focus on the color information, most false-positive samples are caused by the color similarity among many different person images, as shown in Figure 1. By removing the color information, the greyscale branch can enforce the network to pay more attention to other information besides color. For example, in Figure 10, we can observe that the greyscale and RGB branches of the proposed method focus on different regions. The complementarity further demonstrates that greyscale is great in the person Re-ID task.

## 5 CONCLUSION

In this article, we point out that there is a complementarity between RGB and greyscale images in person Re-ID. To fully exploit the information in greyscale and RGB images, we propose a

two-stream network with RGB-grey information. It can effectively combine the color and structure information to produce a robust representation for person Re-ID. The extensive experiments demonstrate not only the superiority of the proposed framework, but also the complementarity between RGB and greyscale images in person Re-ID on four large-scale benchmark datasets. It is hoped that this work can inspire more work on fully exploiting the greyscale information to help feature representation learning in person Re-ID.

## REFERENCES

- [1] Binghui Chen, Weihong Deng, and Jianqi Hu. 2019. Mixed high-order attention network for person re-identification. In *IEEE International Conference on Computer Vision (ICCV'19)*.
- [2] Weihua Chen, Xiaotang Chen, Jianguo Zhang, and Kaiqi Huang. 2017. Beyond triplet loss: A deep quadruplet network for person re-identification. In *IEEE Conference on Computer Vision and Pattern Recognition (CVPR'17)*.
- [3] De Cheng, Yihong Gong, Sanping Zhou, Jinjun Wang, and Nanning Zheng. 2016. Person re-identification by multi-channel parts-based CNN with improved triplet loss function. In *IEEE Conference on Computer Vision and Pattern Recognition (CVPR'16)*.
- [4] Zuozhuo Dai, Mingqiang Chen, Siyu Zhu, and Ping Tan. 2018. Batch feature erasing for person re-identification and beyond. In *IEEE International Conference on Computer Vision (ICCV'19)*.
- [5] Jia Deng, Wei Dong, Richard Socher, Li-Jia Li, Kai Li, and Fei-Fei Li. 2009. ImageNet: A large-scale hierarchical image database. In *IEEE Computer Society Conference on Computer Vision and Pattern Recognition (CVPR'09)*.
- [6] Hehe Fan, Liang Zheng, Chenggang Yan, and Yi Yang. 2018. Unsupervised person re-identification: Clustering and fine-tuning. *ACM Trans. Multimedia Comput. Commun. Applic.* 14, 4 (2018).
- [7] Jianyuan Guo, Yuhui Yuan, Lang Huang, Chao Zhang, Jin-Ge Yao, and Kai Han. 2019. Beyond human parts: Dual part-aligned representations for person re-identification. In *IEEE International Conference on Computer Vision (ICCV'19)*.
- [8] Raia Hadsell, Sumit Chopra, and Yann LeCun. 2006. Dimensionality reduction by learning an invariant mapping. In *IEEE Conference on Computer Vision and Pattern Recognition (CVPR'06)*.
- [9] Kai Han, Jianyuan Guo, Chao Zhang, and Mingjian Zhu. 2018. Attribute-aware attention model for fine-grained representation learning. In *ACM Multimedia Conference on Multimedia Conference (ACM MM'18)*.
- [10] Kaiming He, Xiangyu Zhang, Shaoqing Ren, and Jian Sun. 2016. Deep residual learning for image recognition. In *IEEE Conference on Computer Vision and Pattern Recognition (CVPR'16)*.
- [11] Alexander Hermans, Lucas Beyer, and Bastian Leibe. 2017. In defense of the triplet loss for person re-identification. *arXiv* (2017).
- [12] Ruibing Hou, Bingpeng Ma, Hong Chang, Xinqian Gu, Shiguang Shan, and Xilin Chen. 2019. Interaction-and-aggregation network for person re-identification. In *IEEE Conference on Computer Vision and Pattern Recognition (CVPR'19)*.
- [13] Jie Hu, Li Shen, and Gang Sun. 2018. Squeeze-and-excitation networks. In *IEEE Conference on Computer Vision and Pattern Recognition (CVPR'18)*.
- [14] Mahdi M. Kalayeh, Emrah Basaran, Muhittin Gökmen, Mustafa E. Kamasak, and Mubarak Shah. 2018. Human semantic parsing for person re-identification. In *IEEE Conference on Computer Vision and Pattern Recognition (CVPR'18)*.
- [15] Wei Li, Rui Zhao, Tong Xiao, and Xiaogang Wang. 2014. DeepReID: Deep filter pairing neural network for person re-identification. In *IEEE Conference on Computer Vision and Pattern Recognition (CVPR'14)*.
- [16] Wei Li, Xiatian Zhu, and Shaogang Gong. 2017. Person re-identification by deep joint learning of multi-loss classification. In *Proceedings of the Twenty-Sixth International Joint Conference on Artificial Intelligence (IJCAI'17)*.
- [17] Hao Liu, Jiashi Feng, Meibin Qi, Jianguo Jiang, and Shuicheng Yan. 2017. End-to-end comparative attention networks for person re-identification. *IEEE Trans. Image Proc.* 26, 7 (2017).
- [18] Jinxian Liu, Bingbing Ni, Yichao Yan, Peng Zhou, Shuo Cheng, and Jianguo Hu. 2018. Pose transferrable person re-identification. In *IEEE Conference on Computer Vision and Pattern Recognition (CVPR'18)*.
- [19] Jiawei Liu, Zheng-Jun Zha, Hongtao Xie, Zhiwei Xiong, and Yongdong Zhang. 2018. CA<sub>3</sub>Net: Contextual-attentional attribute-appearance network for person re-identification. In *ACM Multimedia Conference on Multimedia Conference (ACM MM'19)*.
- [20] Lei Qi, Jing Huo, Xiaocong Fan, Yinghuan Shi, and Yang Gao. 2018. Unsupervised joint subspace and dictionary learning for enhanced cross-domain person re-identification. *IEEE J. Select. Topics Sig. Proc.* 12, 6 (2018).
- [21] Lei Qi, Jing Huo, Lei Wang, Yinghuan Shi, and Yang Gao. 2018. MaskReID: A mask based deep ranking neural network for person re-identification. *arXiv* (2018).
- [22] Lei Qi, Lei Wang, Jing Huo, Luping Zhou, Yinghuan Shi, and Yang Gao. 2019. A novel unsupervised camera-aware domain adaptation framework for person re-identification. In *IEEE International Conference on Computer Vision (ICCV'19)*.

- [23] Alec Radford, Luke Metz, and Soumith Chintala. 2016. Unsupervised representation learning with deep convolutional generative adversarial networks. In *International Conference on Learning Representations (ICLR'16)*.
- [24] Ergys Ristani, Francesco Solera, Roger Zou, Rita Cucchiara, and Carlo Tomasi. 2016. Performance measures and a data set for multi-target, multi-camera tracking. In *The European Conference on Computer Vision (ECCV'16)*.
- [25] Jianlou Si, Honggang Zhang, Chun-Guang Li, Jason Kuen, Xiangfei Kong, Alex C. Kot, and Gang Wang. 2018. Dual attention matching network for context-aware feature sequence based person re-identification. In *IEEE Conference on Computer Vision and Pattern Recognition (CVPR'18)*.
- [26] Chunfeng Song, Yan Huang, Wanli Ouyang, and Liang Wang. 2018. Mask-guided contrastive attention model for person re-identification. In *IEEE Conference on Computer Vision and Pattern Recognition (CVPR'18)*.
- [27] Sijie Song, Wei Zhang, Jiaying Liu, and Tao Mei. 2019. Unsupervised person image generation with semantic parsing transformation. In *IEEE Conference on Computer Vision and Pattern Recognition (CVPR'19)*.
- [28] Chi Su, Jianiing Li, Shiliang Zhang, Junliang Xing, Wen Gao, and Qi Tian. 2017. Pose-driven deep convolutional model for person re-identification. In *IEEE International Conference on Computer Vision (CVPR'17)*.
- [29] Yifan Sun, Liang Zheng, Yi Yang, Qi Tian, and Shengjin Wang. 2018. Beyond part models: Person retrieval with refined part pooling (and a strong convolutional baseline). In *The European Conference on Computer Vision (ECCV'18)*.
- [30] Chiat-Pin Tay, Sharmili Roy, and Kim-Hui Yap. 2019. AANet: Attribute attention network for person re-identifications. In *IEEE Conference on Computer Vision and Pattern Recognition (CVPR'19)*.
- [31] Maoqing Tian, Shuai Yi, Hongsheng Li, Shihua Li, Xuesen Zhang, Jianping Shi, Junjie Yan, and Xiaogang Wang. 2018. Eliminating background-bias for robust person re-identification. In *IEEE Conference on Computer Vision and Pattern Recognition (CVPR'18)*.
- [32] Rahul Rama Varior, Bing Shuai, Jiwen Lu, Dong Xu, and Gang Wang. 2016. A Siamese long short-term memory architecture for human re-identification. In *European Conference on Computer Vision (ECCV'16)*.
- [33] Cheng Wang, Qian Zhang, Chang Huang, Wenyu Liu, and Xinggang Wang. 2018. Mancs: A multi-task attentional network with curriculum sampling for person re-identification. In *The European Conference on Computer Vision (ECCV'18)*.
- [34] Longhui Wei, Shiliang Zhang, Wen Gao, and Qi Tian. 2018. Person transfer GAN to bridge domain gap for person re-identification. In *IEEE Conference on Computer Vision and Pattern Recognition (CVPR'18)*.
- [35] Longhui Wei, Shiliang Zhang, Wen Gao, and Qi Tian. 2018. Person transfer GAN to bridge domain gap for person re-identification. In *IEEE Conference on Computer Vision and Pattern Recognition (CVPR'18)*.
- [36] Longhui Wei, Shiliang Zhang, Hantao Yao, Wen Gao, and Qi Tian. 2017. GLAD: Global-local-alignment descriptor for pedestrian retrieval. In *ACM Multimedia Conference on Multimedia Conference (ACM MM'17)*.
- [37] Ancong Wu, Wei-Shi Zheng, Shaogang Gong, and Jianhuang Lai. 2020. RGB-IR person re-identification by cross-modality similarity preservation. *Int. J. Comput. Vis.* 128, 6 (2020).
- [38] Ancong Wu, Wei-Shi Zheng, Hong-Xing Yu, Shaogang Gong, and Jianhuang Lai. 2017. RGB-infrared cross-modality person re-identification. In *IEEE International Conference on Computer Vision (ICCV'17)*.
- [39] Tong Xiao, Hongsheng Li, Wanli Ouyang, and Xiaogang Wang. 2016. Learning deep feature representations with domain guided dropout for person re-identification. In *IEEE Conference on Computer Vision and Pattern Recognition (CVPR'16)*.
- [40] Wenjie Yang, Houjing Huang, Zhang Zhang, Xiaotang Chen, Kaiqi Huang, and Shu Zhang. 2019. Towards rich feature discovery with class activation maps augmentation for person re-identification. In *IEEE Conference on Computer Vision and Pattern Recognition (CVPR'19)*.
- [41] Dong Yi, Zhen Lei, Shengcai Liao, and Stan Z. Li. 2014. Deep metric learning for person re-identification. In *International Conference on Pattern Recognition (ICPR'14)*.
- [42] Quan Zhang, Haijie Cheng, Jianhuang Lai, and Xiaohua Xie. 2019. DHML: Deep heterogeneous metric learning for VIS-NIR person re-identification. In *Chinese Conference on Biometric Recognition (CCBR'19)*.
- [43] Haiyu Zhao, Maoqing Tian, Shuyang Sun, Jing Shao, Junjie Yan, Shuai Yi, Xiaogang Wang, and Xiaou Tang. 2017. Spindle Net: Person re-identification with human body region guided feature decomposition and fusion. In *IEEE Conference on Computer Vision and Pattern Recognition (CVPR'17)*.
- [44] Yiru Zhao, Xu Shen, Zhongming Jin, Hongtao Lu, and Xian-sheng Hua. 2019. Attribute-driven feature disentangling and temporal aggregation for video person re-identification. In *IEEE Conference on Computer Vision and Pattern Recognition (CVPR'19)*.
- [45] Liang Zheng, Liyue Shen, Lu Tian, Shengjin Wang, Jingdong Wang, and Qi Tian. 2015. Scalable person re-identification: A benchmark. In *IEEE International Conference on Computer Vision (CVPR'15)*.
- [46] Meng Zheng, Srikrishna Karanam, Ziyan Wu, and Richard J. Radke. 2019. Re-identification with consistent attentive siamese networks. In *IEEE Conference on Computer Vision and Pattern Recognition (CVPR'19)*.
- [47] Zhedong Zheng, Xiaodong Yang, Zhiding Yu, Liang Zheng, Yi Yang, and Jan Kautz. 2019. Joint discriminative and generative learning for person re-identification. In *IEEE Conference on Computer Vision and Pattern Recognition (CVPR'19)*.

- [48] Zhedong Zheng, Liang Zheng, and Yi Yang. 2017. Unlabeled samples generated by GAN improve the person re-identification baseline in vitro. In *IEEE International Conference on Computer Vision (ICCV'17)*.
- [49] Zhedong Zheng, Liang Zheng, and Yi Yang. 2018. A discriminatively learned CNN embedding for person reidentification. *ACM Trans. Multimedia Comput. Commun. Applic.* 14, 1 (2018).
- [50] Zhun Zhong, Liang Zheng, Donglin Cao, and Shaozi Li. 2017. Re-ranking person re-identification with k-reciprocal encoding. In *IEEE Conference on Computer Vision and Pattern Recognition (CVPR'17)*.
- [51] Zhun Zhong, Liang Zheng, Guoliang Kang, Shaozi Li, and Yi Yang. 2017. Random erasing data augmentation. In *Proceedings of the AAAI Conference on Artificial Intelligence (AAAI'20)*.
- [52] Zhun Zhong, Liang Zheng, Shaozi Li, and Yi Yang. 2018. Generalizing a person retrieval model hetero-and homogeneously. In *The European Conference on Computer Vision (ECCV'18)*.
- [53] Zhun Zhong, Liang Zheng, Zhedong Zheng, Shaozi Li, and Yi Yang. 2018. Camera style adaptation for person re-identification. In *IEEE Conference on Computer Vision and Pattern Recognition (CVPR'18)*.

Received August 2019; revised April 2020; accepted August 2020